COPPER OXIDE NANORODS BASED NANOFIBERS MEMBRANE FOR SOLAR-DRIVEN INTERFACIAL EVAPORATION

by

Jiang-Hui ZHAO[a,b], Bing GAO[b], Jun-Xian HONG[b], Siew Chun LOW[a], Zhen-Zhen XU[b], and Soon Huat TAN[a*]*

[a] School of Chemical Engineering, Engineering Campus, University Sains Malaysia,
Seri Ampangan, Nibong Tebal, Pulau Pinang, Malaysia
[b] School of Textile and Garment, Anhui Polytechnic University, Wuhu, China

Solar-driven interfacial evaporation system has attracted intensive attention owing to its great potential in harnessing renewable solar energy to purify water. To further enhance the solar-driven interfacial evaporation system performance, solar absorber structure with high light-thermal energy conversion efficiency is especially critical. In this work, polyvinyl pyrrolidone/poly(vinylidene fluoride co hexa fluoropropylene)/CuO-nanorods (PVP/PVDF-HFP/CuO-nanorods) membrane was prepared sequentially by electrospinning, heating and hydrothermal processes. The flexible electrospun membrane was used as the photothermal layer in the solar-driven interfacial evaporation system. The evenly distributed CuO nanorods function as solar energy absorbers. The polystyrene foam was used as an insulating layer, and filter paper was inserted in the middle of the polystyrene foam to transport water to the photothermal layer. The designed evaporator was used for the solar evaporation using pure water. As a result, the evaporation rate was 1.11 kg/m²h and the light-thermal energy conversion rate was 75.36%. The outcome of this work provides the potential of solar-driven interfacial evaporation system for water desalination and wastewater purification.

Key words: *solar-driven interfacial evaporation, electrospinning, hydrothermal, copper nanorods*

Introduction

Nowadays, energy crisis has become a critical issue caused by population growth, industrial growth, and continued dependence on fossil fuels [1, 2]. As conventional fossil fuels become scarce and expensive [3], efforts to explore renewable energy are one of the ways to meet the continuing growth in energy demand. Among RES such as solar, wind, hydropower, geothermal, and bioenergy [4], solar energy seems to be the best option for the future world because it is reliable, abundant, cost-effective, ecosystem friendly, and durable [5]. Currently, the three main strategies for harnessing solar energy are photovoltaic, solar chemistry, and solar thermal conversion [6]. Among them, solar thermal conversion is a direct method to transform sunlight energy into thermal energy using photothermal materials [7]. Solar driven evaporation is a typical example of solar thermal conversion application.

Solar driven evaporation, which utilizes sunlight as an energy source to produce fresh water from seawater, wastewater or polluted water, not only alleviates the energy crisis, but also provides an alternative strategy to resolve the severe situation of water scarcity [8, 9]. Depending on the location of the photothermal material, three different solar driven evaporation systems exist: bottom evaporation system, volumetric system, and interfacial system [10]. In bottom and volumetric systems, the entire bulk water is heated to produce steam, therefore, a large amount of thermal energy is lost in the water. However, in the solar driven interfacial evaporation (SDIE) system, the photothermal material is directly placed on the water surface, and the converted thermal energy is directly used to heat the water molecules at the air-water surface, thereby reducing the thermal energy transfer to the bulk water [11, 12].

Electrospinning is one of the methods to fabricate membrane for SDIE system [13]. Electrospun membranes can be obtained by the electrospinning or the bubble electrospinning [14-17], which have many advantages, and typically exhibit more than 90% porosity at controlled thicknesses. The abundant pore structure facilitates the transport of water from the bulk water to the surface and prevents heat dissipation from the surface to the bulk water [18]. Besides, the membrane size, thickness, and porosity can be adjusted by controlling the electrospinning parameters [19, 20]. Meanwhile, the electrospun membranes are flexible, can be customized and easy for transportation, making them convenient and portable for practical applications [21].

In electrospun membrane-based SDIE systems, photothermal materials play a critical role in absorbing solar energy [22]. In this work, CuO nanorods were used as the photothermal materials. The PVP/PVDF-HFP/CuO-nanorods nanofibers membrane was prepared through core-shell electrospinning, heating and hydrothermal processes. After the hydrothermal process, CuO nanorods were uniformly formed along the core of PVDF-HFP nanofibers. This work aims to demonstrate the potential photothermal ability of CuO nanorods in SDIE system.

Experimental

Materials

Poly(vinylidene fluoride-co-hexa-fluoropropylene) (PVDF-HFP, molecular weight (MW 400,000), Polyvinylpyrrolidone (PVP, MW 1,300,000) and cupric acetate anhydrous ($Cu(CH_3COO)_2$) were purchased from Aladdin Industrial Corporation, (Shanghai, China). N, N-dimethyl formamide (DMF), acetone, and ammonia were supplied by Sinopharm Chemical Reagent Co., Ltd. (Suzhou, China). Absolute ethanol was supplied by Prospect Chemical Reagents Co., Ltd. (Wuxi, China). All reagents were analytical grade and used as received without further purification.

Preparation of PVP/PVDF-HFP/Cu(CH₃COO)₂ nanofibers
membrane by core-shell electrospinning process

The PVDF-HFP (16 wt.%) was dissolved in a binary solvent of acetone/DMF (weight ratio of 1:4) at room temperature for four hours using a magnetic stirrer. Then the cupric acetate was added to the prepared PVDF-HFP solution, and the weight ratio of cupric acetate anhydrous/PVDF-HFP was 1:4. The mixed solution was then stirred for 20 minutes at 70 ℃ to form a blue shell solution. Meanwhile, PVP (8 wt.%) was dissolved in ethanol to form the core solution. During core-shell electrospinning process, the collector distance was kept at 17 cm and a voltage of 20 kV was applied. The core flow rate of PVP was 0.4 mL per

hour and the shell flow rate was 0.6 mL per hour. The ambient relative humidity and temperature were 50 ±2% and 25 ±2 ℃, respectively.

Preparation of PVP/PVDF-HFP/CuO-seed nanofibers membrane by heating process

The as-prepared PVP/PVDF-HFP/Cu(CH$_3$COO)$_2$ nanofibers membrane was placed in an oven with excess deionized water in a large beaker for 20 hours at 120 ℃. The Cu(CH$_3$COO)$_2$ on the nanofibers were then converted into CuO, which served as seed for the nucleation and crystallization of CuO nanorods in subsequent steps.

Preparation of PVP/PVDF-HFP/CuO-nanorods nanofibers membrane by hydrothermal process

The growth media solution was prepared by 50 g deionized water, 1.5 g cupric acetate anhydrous, and excess ammonia. The heat-treated PVP/PVDF-HFP/CuO nanofibers membrane was then immersed in the growth solution contained by the hydrothermal reactor. The reactor was placed in an oven for 10 hours at 90 ℃. Then, the resultant membrane was rinsed with deionized water and dried in an oven to remove water residues.

Characterization

The morphologies of nanofiber membranes were observed via SEM (Hitachi S-4800, Japan) apparatus.

Interfacial solar-driven evaporation experiments

In the interfacial solar-driven evaporation experiment, deionized water was placed in a small 100 mL beaker. A piece of polystyrene (PS) foam floats on the water to support the PVP/PVDF-HFP/CuO-nanorods nanofibers membrane. A commercially available filter paper was inserted in the middle of the polystyrene foam to transport water to the photothermal layer. The whole system was irradiated under a solar simulator (PL-XQ500W, Xenon light source, Beijing Precise Technology co., Ltd.) with an illumination of 1000 W/m^2 (1 sun). Mass changes throughout the sample were recorded in real time using a precision balance (FX-3000i, 0.01 g, A&D Company, Limited.) connected to a computer. An infrared thermal imager (FLIR C5, FLIR Systems Inc., USA) was used to record the temperature changes of the samples. For comparison, a system consisting of PS foam and filter paper in pure water without PVP/PVDF-HFP/CuO-nanorods nanofibers membrane was used as a blank control.

Results and discussion

Morphology of the membranes

As shown in figs. 1(a) and 1(d), the morphology of PVP/PVDF-HFP/Cu(CH$_3$COO)$_2$ nanofibers after core shell electrospinning was smooth with an average diameter of 196 nm. After heat treatment, the morphologies of the PVP/PVDF-HFP/CuO nanofibers, figs. 1(b) and 1(e) were still smooth, but the diameter was decreased to an average of 139 nm. This can be attributed to fiber shrinking and remodeling during solvent evaporation in the heating process [21]. After hydrothermal treatment, CuO nanorods with a length of about 145 nm and a diameter of about 35 nm, figs. 1(c) and 1(f) were grew uniformly along the nanofibers. Finally, the furry appearance of PVP/PVDF-HFP/CuO-nanorods nanofibers yield an average diameter of 362 nm.

1988

Zhao, J.-H., *et al.*: Copper Oxide Nanorods Based Nanofibers Membrane for …
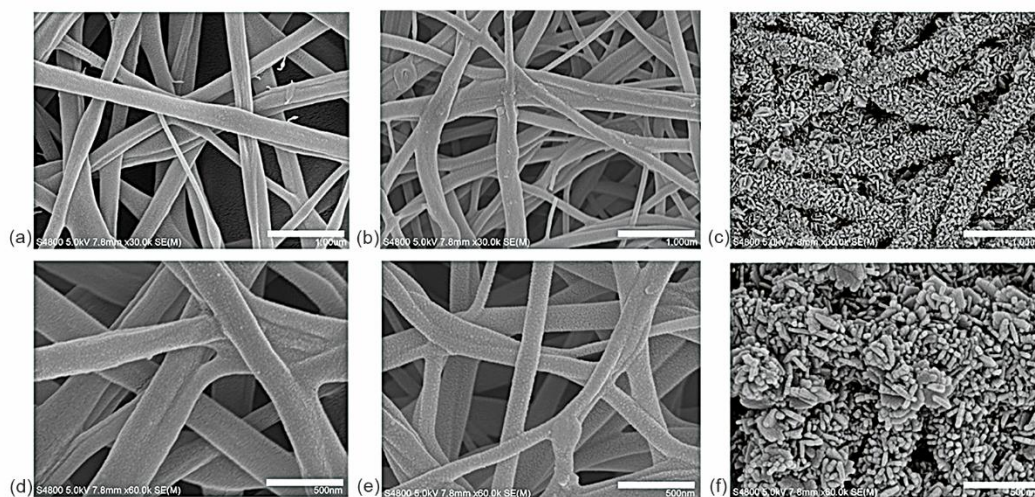THERMAL SCIENCE: Year 2023, Vol. 27, No. 3A, pp. 1985-1991

Figure 1. The SEM images of PVP/PVDF-HFP/Cu(CH₃COO)₂ nanofibers membrane after core-shell electrospinning (a) and (d), PVP/PVDF-HFP/CuO nanofibers membrane after heat treatment (b) and (e), and PVP/PVDF-HFP/CuO-nanorods nanofibers membrane after hydrothermal treatment (c) and (f)

Infrared thermal imaging monitoring

Figures 2 and 3 show infrared thermal images during the experiment from top and side views, respectively. It can be seen from fig. 2 that the surface temperatures of the blank control system and SDIE system were 27.8 °C and 29.6 °C, respectively, at the onset of solar evaporation, figs. 2(a) and 2(d). After 5 minutes of solar evaporation process, both blank control system and SDIE system showed rapid heating capability, reaching 30.9 °C and 31.3 °C, respectively, figs. 2(b) and 2(e). After a longer period of solar evaporation (60 minutes), a more stable temperature was observed for the blank control system, 30.2 °C, fig. 2(c), and SDIE system, 33.6 °C, fig. 2(f). Generally, the SDIE system showed higher temperature than
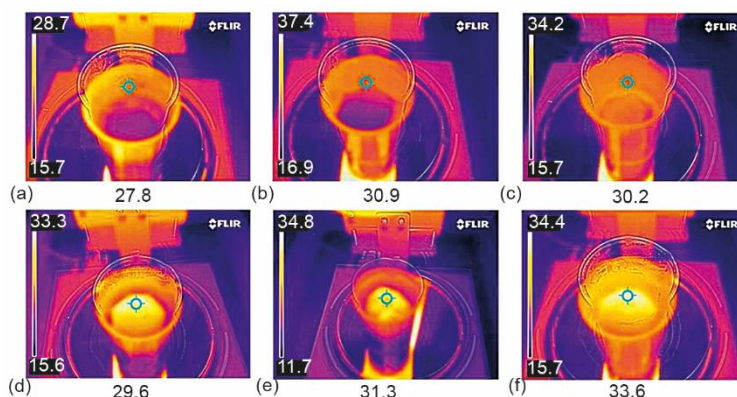

Figure 2. Infrared thermal images of top surfaces of the solar evaporation experiment for the (a)-(c) blank control system without PVP/PVDF-HFP/CuO-nanorods membrane and (d)-(f) SDIE system with PVP/PVDF-HFP/CuO-nanorods membrane at 0, 5, and 60 minutes, respectively

Zhao, J.-H., *et al.*: Copper Oxide Nanorods Based Nanofibers Membrane for …
THERMAL SCIENCE: Year 2023, Vol. 27, No. 3A, pp. 1985-1991

1989

the blank control system due to the photothermal capability of the PVP/PVDF-HFP/CuO-nanorods membrane and the good thermal conductivity of CuO on the membrane surface. The increase in temperature will favor the transition of water from liquid to vapor phase, which enables the SDIE system to achieve higher evaporation rate and efficiency. In contrast, at the end of the experiment, the side view temperature of the blank control system, 27.6 °C, fig. 3(c) was higher than that of the SDIE system, 26.2 °C, fig. 3(f). This is due to better thermal management of the SDIE system using PVP/PVDF-HFP/CuO-nanorods membrane.
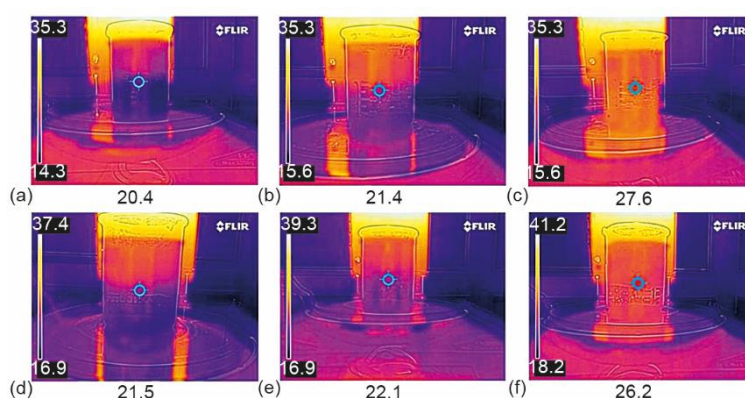

Figure 3. Infrared thermal images of side view of the solar evaporation experiment for the (a)-(c) blank control system without PVP/PVDF-HFP/CuO-nanorods membrane and (d)-(f) SDIE system with PVP/PVDF-HFP/CuO-nanorods membrane at 0, 5, and 60 minutes, respectively

Water weight monitoring in the solar evaporation experiment

Figure 4 shows the mass change of the SDIE system with and without the PVP/PVDF-HFP/CuO-nanorods membrane in the solar evaporation experiment. The SDIE system with PVP/PVDF-HFP/CuO-nanorods membrane showed higher water evaporation rate compared to the blank control system. Within one hour, the mass loss of the blank control system and SDIE systems were 1.96 g, 3.14 g, respectively.

Figure 4. Mass change in the solar evaporation experiment; (a) blank control system without the PVP/PVDF-HFP/CuO-nanorods membrane and (b) SDIE system composed of the PVP/PVDF-HFP/CuO-nanorods membrane
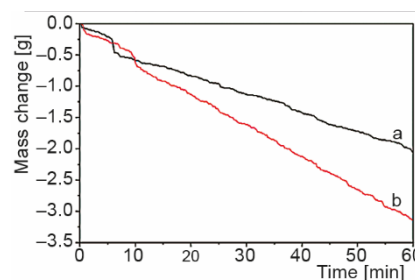
Two vital parameters to quantify the water evaporation process are evaporation rate, *m*, and evaporation efficiency, *η*. It can be calculated using the following equations:

$$m = \frac{m_{loss}}{\dfrac{\pi}{4D^2 t}} \tag{1}$$

1990

Zhao, J.-H., *et al.*: Copper Oxide Nanorods Based Nanofibers Membrane for …
THERMAL SCIENCE: Year 2023, Vol. 27, No. 3A, pp. 1985-1991

$$\eta = \frac{mh}{q} \qquad (2)$$

$$h = C_m \Delta T + 1.91846 \cdot 10^3 \left(\frac{T}{T - 33.91} \right)^2 \qquad (3)$$

where m_{loss} is the water mass loss in the evaporation experiment, D – the diameter of the membrane ($D = 60$ mm), t – the the evaporation duration time ($t = 1$ hour), q – the solar intensity ($q = 1000$ W/m^2), h [Jg^{-1}] – the total enthalpy change consists of sensible heat for temperature rise and the latent heat for phase change, C_m – the specific heat capacity of water ($C_m = 4.18$ J/gK), ΔT – the increment temperature of water [(273.15 + 33.6) – – (273.15 + 29.6) = 4 K], and T – the final temperature (36 °C, 306.75 K).

As a result, the evaporation rate, m, and evaporation efficiency, η, of the SDIE system were 1.11 kg/m^{2}h and 75.36%, respectively. On the other hand, for the blank control system, the evaporation rate, m, and evaporation efficiency, η, were 0.69 kg/m^{2}h and 47.06%, respectively. Obviously, the SDIE system with PVP/PVDF-HFP/CuO-nanorods membrane achieves improved performance. This is due to the CuO nanorods exhibiting higher solar energy absorption capacity and superhydrophilicity, which contribute to higher evaporation rate and evaporation efficiency.

Conclusion

In this work, a SDIE system was designed to verify its performance in solar driven evaporation. The SDIE system consists of a photothermal layer of electrospun PVP/PVDF-HFP/CuO-nanorods nanofibers membrane, a thermal insulating PS foam, and a filter paper as a water wicking material inserted into the center of the PS foam. For the photothermal layer, PVP/PVDF-HFP/CuO-nanorods nanofibers membrane was innovatively fabricated using core-shell electrospinning, heating and hydrothermal processes. The PVP/PVDF-HFP/CuO-nanorods nanofibers membrane demonstrated good photothermal ability. In a pure water solar evaporation experiment, a relatively high evaporation rate of 1.11 kg/m^{2}h and a light-thermal energy conversion rate of 75.36% were achieved. This work demonstrates the potential photothermal ability of CuO in solar driven evaporation and will stimulate more research on the use of semiconductor photothermal materials.

Acknowledgment

References

[1] Singh, S., Energy Crisis and Climate Change: Global Concerns and Their Solutions, *Energy: Crises, Challenges and Solutions,* On-line first, https://doi.org/10.1002/9781119741503, ch1, 2021
[2] Kanwal, S., *et al*., An Integrated Future Approach for the Energy Security of Pakistan: Replacement of Fossil Fuels with Syngas for Better Environment and Socio-Economic Development, *Renewable and Sustainable Energy Reviews, 156* (2022), Mar., pp. 111978
[3] Zamparas, M., The Role of Resource Recovery Technologies in Reducing the Demand of Fossil Fuels and Conventional Fossil-Based Mineral Fertilizers, in: *Low Carbon Energy Technologies in Sustainable Energy Systems,* Elsevier, Amsterdam, The Nederlands, 2021, pp. 3-24

[4] Yao, Y., *et al.*, Untangling Global Levelised Cost of Electricity Based on Multi-Factor Learning Curve for Renewable Energy: Wind, Solar, Geothermal, Hydropower and Bioenergy, *Journal of Cleaner Production, 285* (2021), Feb., pp. 124827

[5] Danish, M. S. S., *et al.*, Photocatalytic Applications of Metal Oxides for Sustainable Environmental Remediation, *Metals, 11* (2021), 1, 80

[6] Wu, D., *et al.,* Solar Evaporation and Electricity Generation of Porous Carbonaceous Membrane Prepared by Electrospinning and Carbonization, *Solar Energy Materials and Solar Cells, 215* (2020), Sept., 110591

[7] Li, W., *et al.*, Self-Encapsulating Ag Nanospheres in Amorphous Carbon: A Novel Ultrathin Selective Absorber for Flexible Solar-Thermal Conversion, *Journal of Materials Chemistry A, 9* (2021), 18, pp. 11300-11311

[8] Wang, J., *et al.,* Hexagonal Cluster Mn-MOF Nanoflowers with Super-Hydrophilic Properties for Efficient and Continuous Solar-Driven Clean Water Production, *Sustainable Energy & Fuels, 5* (2021), 7, pp. 1995-2002

[9] Ding, T., *et al.*, Hybrid Solar-Driven Interfacial Evaporation Systems: Beyond Water Production Towards High Solar Energy Utilization, *Materials Today, 42* (2021), Jan.-Feb., pp. 178-191

[10] Liu, X., *et al.*, Towards Highly Efficient Solar-Driven Interfacial Evaporation for Desalination, *Journal of Materials Chemistry A, 8* (2020), 35, pp. 17907-17937

[11] Sheng, M., *et al.,* Recent Advanced Self-Propelling Salt-Blocking Technologies For Passive Solar-Driven Interfacial Evaporation Desalination Systems, *Nano Energy Part B, 89* (2021), Nov., pp. 106468

[12] Sun, H., *et al.*, Facile Preparation of a Carbon-Based Hybrid Film for Efficient Solar-Driven Interfacial Water Evaporation, *ACS Applied Materials & Interfaces, 13* (2021), 28, pp. 33427-33436

[13] Li, D., *et al.*, A Flexible and Salt-Rejecting Electrospun Film-Based Solar Evaporator For Economic, Stable and Efficient Solar Desalination And Wastewater Treatment, *Chemosphere, 267* (2021), Mar., 128916

[14] Qian, M., He, J., Collection of Polymer Bubble as a Nanoscale Membrane, *Surfaces and Interfaces, 28* (2022), Feb., 101665

[15] He, J., *et al.*, The Maximal Wrinkle Angle During the Bubble Collapse and Its Application to the Bubble Electrospinning, *Frontiers in Materials, 8* (2022), 800567

[16] Liu, L., *et al.*, Dropping in Electrospinning Process: A General Strategy for Fabrication of Microspheres, *Thermal Science, 25* (2021), 2B, pp. 1295-1303

[17] Lin, L., *et al.,* Fabrication of PVDF/PES Nanofibers with Unsmooth Fractal Surfaces by Electrospinning: A General Strategy and Formation Mechanism, *Thermal Science, 25* (2021), 2B, pp. 1287-1294

[18] Liu, Y., *et al.*, Bioinspired Design of Electrospun Nanofiber Based Aerogel for Efficient and Cost-Effective Solar Vapor Generation, *Chemical Engineering Journal, 427* (2022), Jan., 131539

[19] Liu, Z., *et al.*, Electrospun Jets Number and Nanofiber Morphology Effected by Voltage Value: Numerical Simulation and Experimental Verification, *Nanoscale Research letters, 14* (2019), 1, pp. 1-9

[20] Gao, K., *et al.,* Co-N-Doped Directional Multichannel PAN/CA-Based Electrospun Carbon Nanofibers as High-Efficiency Bifunctional Oxygen Electrocatalysts for Zn-Air Batteries, *ACS Sustainable Chemistry & Engineering, 9* (2021), 50, pp. 17068-17077

[21] Liu, Z., *et al.*, Superflexible/Superhydrophilic PVDF-HFP/CuO-Nanosheet Nanofibrous Membrane for Efficient Microfiltration, *Applied Nanoscience, 9* (2019), 8, pp. 1991-2000

[22] Pan, J., *et al.*, Diatom-Inspired TiO_2-PANi-Decorated Bilayer Photothermal Foam for Solar-Driven Clean Water Generation, *ACS Applied Materials & Interfaces, 13* (2021), 48, pp. 58124-58133